

# Learning Contour-Guided 3D Face Reconstruction with Oclusions

Dapeng Zhao<sup>a</sup>

<sup>a</sup>*Zhejiang Lab, Hangzhou, China*

---

## Abstract

3D face reconstruction is a versatile technology applied in various contexts. Deep learning methods, in particular, prove highly valuable in this domain due to their ability to generate high-quality 3D models. Nevertheless, most of these techniques require unobstructed and clear facial images as input. In response, we've developed a 3D face reconstruction system capable of performing effectively even when faced with obstructed views. Taking inspiration from generative face image inpainting, we've introduced a comprehensive method for crafting facial representations guided by their outlines. Our network comprises two components: one dedicated to image enhancement by removing obstructions and restoring missing facial features, while the other utilizes weak supervision to craft exceptionally detailed 3D models. Through extensive experimentation on standard 3D face reconstruction tasks, we've demonstrated the superiority of our method compared to existing ones that often fall short. Our results, based on experiments conducted with LFW databases, affirm the effectiveness of our approach.

*Keywords:* 3D Reconstruction, Face Parsing, Face Recognition

---

## 1. Introduction

Face reconstruction systems find extensive applications in specific scenarios, including face recognition [Banz and Vetter \(2003\)](#) and digital entertainment [Cao et al. \(2014\)](#). Nonetheless, the majority of these systems require the input face photos to be unobstructed and depict the front of the face. In contrast to recent research efforts focused on enhancing facial resolution and fidelity [Lin et al. \(2020\)](#), 3D face reconstruction in occluded environments remains underexplored. Consequently, addressing the challenge of reconstructing faces in obstructed scenes is a pressing task.

Face images can be occluded by anything, such as palms, glasses, or leaves. Without any prior or weak supervision, it has been shown that we cannot simply infer the occluded face image. However, face image synthesis has achieved tremendous success in recent years due to the rapid development of Generative Adversarial Networks (GANs). State-of-the-art GAN techniques, such as Stylegan2 [Karras et al. \(2020\)](#), can generate high-fidelity virtual face images that are sometimes even difficult to distinguish from real ones.

In this work, we investigated the identification of occluded areas and the removal of oclusions to synthesize a complete face from a human face. We used face parsing networks to identify the occluded areas and used a contour-based GAN to synthesize a complete 2D face. Due to the lack of 3D datasets, we utilized a weakly supervised deep learning framework to predict the coefficients of the 3D Morphable Model (3DMM). In the end, we obtained the final face model with complete facial features.

*This research makes three contributions:*

- We propose an algorithm that combines face analysis map and face contour map to generate face with full facial features.
- We have improved the loss function of our 3D reconstruction framework for occluded scenes. Our results are more accurate than other state-of-the-art methods.
- We propose a novel 3D face reconstruction method that can produce accurate models under occluded scenes.

---

*Email address:* [mirror1775@gmail.com](mailto:mirror1775@gmail.com) (Dapeng Zhao)

## 2. Related Work

### 2.1. Generic Face Reconstruction

Deep learning-based methods [Tuan Tran et al. \(2017\)](#) directly regress 3D Morphable Model (3DMM) coefficients from images. Some frameworks [Jourabloo and Liu \(2016\)](#) have explored end-to-end convolutional neural network (CNN) architectures to regress 3DMM coefficients directly. However, most of these methods require that the input image is an unobstructed frontal face. In order to obtain paired 2D-3D data for supervised learning, these approaches typically require very deep CNNs, which can be difficult to train. Additionally, these approaches do not perform well when dealing with complex lighting, occlusion, and other in-the-wild conditions.

### 2.2. Face Parsing

Face parsing maps are commonly used as an essential intermediate representation for generative modeling [Johnson et al. \(2018\)](#). They can be used as the conditional context for conditional face image synthesis. Image-to-image translation models can learn the mapping from parsing maps to realistic RGB images [Isola et al. \(2017\)](#). A practical face parsing solution should directly predict per-pixel semantic labels across the entire face image. To obtain accurate parsing maps, [Wei et al. \(2017\)](#) developed a novel method for regulating receptive fields with superior regulation ability in parsing networks. MaskGan [Lee et al. \(2020\)](#) provided a labeled face parsing dataset. [Zhao et al. \(2017\)](#) developed a model that explored how to combine the fully convolutional network and super-pixels data. To address the problem of limited access to global image information, some methods [Yin et al. \(2021\)](#) have introduced the transformer component. Semantic layouts provide rough guidance of the location and appearance of objects, which further facilitates training.

### 2.3. Face Image Synthesis

Due to the rapid development of convolutional neural networks, deep pixel-level face generation has shown extraordinary capabilities. Recently, several methods have been introduced that provide additional information before face image synthesis. One of the first deep learning methods designed for image inpainting is context encoder [Pathak et al. \(2016\)](#), which uses an encoder-decoder framework. However, the network performs poorly on human faces. Following this work, [Dolhansky et al. \(2018\)](#) demonstrated the importance of exemplar data for inpainting. However, this method only focuses on filling in missing eye regions of frontal faces, so it does not generalize well. In subsequent work, a pre-trained VGG network was used to improve the output of the context encoder by minimizing the feature differences between the input image and the inpainted image [Yang et al. \(2017\)](#).

In the face synthesis task, the encoder converts an image with the concerned regions into a low-dimensional feature space. The decoder then builds the output image. However, due to the data bottleneck in the channel-wise fully connected layer, the restored regions of the output image often contain visual artifacts and appear blurry. [Iizuka et al. \(2017\)](#) solved this problem by replacing the fully connected layer with a series of dilated convolutional layers. [Yu et al. \(2018\)](#) proposed a two-step image synthesis method. In the first step, it estimates the missing area in a coarse manner. The refinement network then uses an attention mechanism to sharpen the result by looking for a collection of background patches with the highest similarity to the coarse estimate.

## 3. Proposed Approach

We propose a 3D face reconstruction method based on a single image (as shown in Figure 1). The method consists of two stages. The first stage, face image synthesis under occluded scenes, synthesizes a complete face image from an occluded image. The second stage, a 3D face reconstruction network based on unobstructed frontal images, reconstructs a 3D face model from the synthesized complete face image. Our goal is to realize 3D face reconstruction under occluded scenes using this framework. Given a source image  $\mathbf{I}_{\text{input}} \in \mathbb{R}^{H \times W \times 3}$  with obstructions on the face, we obtain the final face model.

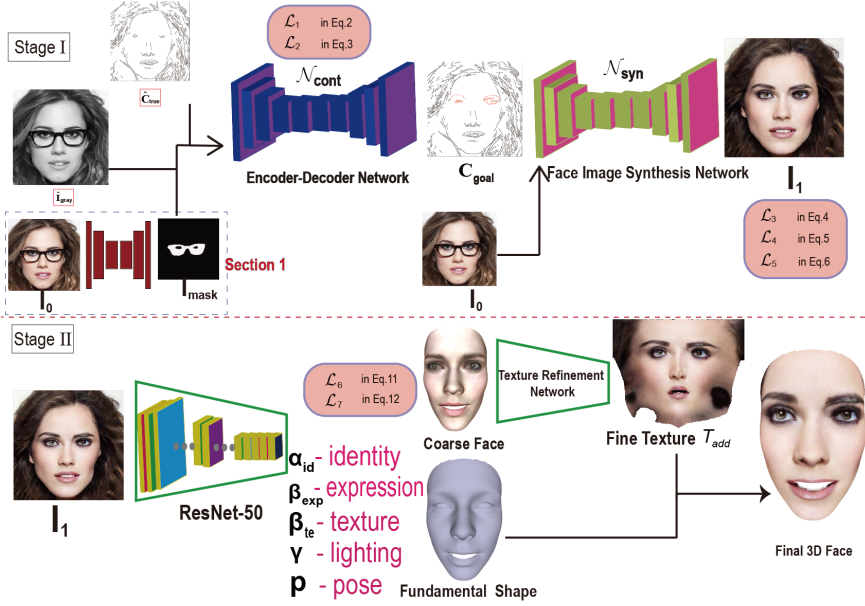


Figure 1: Method overview. See related sections for details.

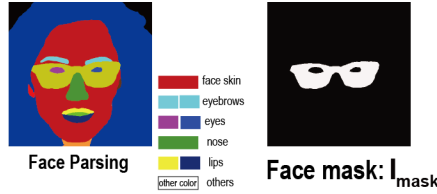


Figure 2: The face mask we define, indicating the position of the occlusions.

### 3.1. How to Obtain the Face Mask

As show in Section 1 of Figure 1 and Figure 2, we define face mask image  $\mathbf{I}_{\text{mask}} \in \mathbb{R}^{H \times W \times 1}$  (1 for the occluded occlusions, 0 for background) indicating the position of the occlusions. Our face mask  $\mathbf{I}_{\text{mask}}$  and traditional face parsing map are closely related. We need to separate the facial features, and we can reveal the area of the occlusions. Please notice that, in our work, we assumed that facial features only include only five parts, including facial skin, eyebrows, eyes, nose and lips. Inspired by the method of CelebAMask-HQ Lee et al. (2020), given an input face image  $\mathbf{I}_0 \in \mathbb{R}^{H \times W \times 3}$  under extreme scenes, we leveraged an encoder-decoder module  $\Omega_m$  based on U-Net to obtain the face mask.

### 3.2. Complete Face Image Generation

Our image synthesis module is guided by the contour (some approaches called *edge*). First, we need to predict the contours  $\mathbf{C}_{\text{syn}} \in \mathbb{R}^{H \times W \times 1}$  of facial features in the occluded area. We assume that the final unobstructed face image is  $\mathbf{I}_1 \in \mathbb{R}^{H \times W \times 3}$  and the ground truth image without obstruction  $\mathbf{I}_{\text{true}} \in \mathbb{R}^{H \times W \times 3}$ . In the training set, the corresponding complete contour image and gray image are  $\mathbf{C}_{\text{true}} \in \mathbb{R}^{H \times W \times 1}$  and  $\mathbf{I}_{\text{gray}} \in \mathbb{R}^{H \times W \times 1}$ . We trained the contour generator  $\mathcal{N}_{\text{cont}}$  to predict the contour map for the occluded region

$$\begin{cases} \mathbf{C}_{\text{syn}} = \mathcal{N}_{\text{cont}}(\hat{\mathbf{I}}_{\text{gray}}, \mathbf{I}_{\text{mask}}, \hat{\mathbf{C}}_{\text{true}}) \\ \hat{\mathbf{I}}_{\text{gray}} = \mathbf{I}_{\text{gray}} \odot (1 - \mathbf{I}_{\text{mask}}) \\ \hat{\mathbf{C}}_{\text{true}} = \mathbf{C}_{\text{true}} \odot (1 - \mathbf{I}_{\text{mask}}) \end{cases} \quad (1)$$

where  $\hat{\mathbf{I}}_{\text{gray}}$  denotes masked grayscale image,  $\hat{\mathbf{C}}_{\text{true}}$  denotes masked contour image and  $\odot$  denotes the Hadamard product.

We trained the discriminator of the module  $\mathcal{N}_{\text{cont}}$  to predict which of  $\mathbf{C}_{\text{syn}}$  and  $\mathbf{C}_{\text{true}}$  is true contour map and which is false contour map. The adversarial loss is defined as

$$\begin{aligned} \mathcal{L}_1 = & \mathbb{E}_{(\mathbf{C}_{\text{true}}, \mathbf{I}_{\text{gray}})} [\log D_1(\mathbf{C}_{\text{true}}, \mathbf{I}_{\text{gray}})] \\ & + \mathbb{E}_{(\mathbf{I}_{\text{gray}})} \log [1 - D_1(\mathbf{C}_{\text{syn}}, \mathbf{I}_{\text{gray}})] \end{aligned} \quad (2)$$

In addition, we compare the feature activation maps of the discriminator. We set the face feature matching loss as

$$\mathcal{L}_2 = \mathbb{E} \left[ \sum_{i=1}^K \frac{1}{N_i} \left\| D_1^{(i)}(\mathbf{C}_{\text{true}}) - D_1^{(i)}(\mathbf{C}_{\text{syn}}) \right\| \right] \quad (3)$$

where  $N_i$  is the number of elements in the  $i$ th activation layer,  $K$  is the final convolution layer of the discriminator and  $D_1^{(i)}$  is the activation in the  $i$ th layer of the discriminator.

After obtaining the complete contour map, we design  $\mathcal{N}_{\text{syn}}$  to generate the complete face image  $\mathbf{I}_1$ . The complete contour map  $\mathbf{C}_{\text{goal}}$  is formed by adding  $\mathbf{C}_{\text{syn}}$  and  $\mathbf{C}_{\text{true}}$ , which follows  $\mathbf{C}_{\text{goal}} = \mathbf{C}_{\text{true}} \odot (1 - \mathbf{I}_{\text{mask}}) + \mathbf{C}_{\text{syn}} \odot \mathbf{I}_{\text{mask}}$ . In the map  $\mathbf{C}_{\text{goal}}$ , we can see the contours of all facial features, especially the occluded areas. In addition, we set  $\hat{\mathbf{I}}_{\text{true}} \in \mathbb{R}^{H \times W \times 3}$  to be an incomplete face picture, which follows  $\hat{\mathbf{I}}_{\text{true}} = \mathbf{I}_{\text{true}} \odot (1 - \mathbf{I}_{\text{mask}})$ . So, we utilize  $\mathcal{N}_{\text{syn}}$  to get the final complete face image  $\mathbf{I}_1$ , with occluded regions recovered, which follows  $\mathbf{I}_1 = \mathcal{N}_{\text{syn}}(\hat{\mathbf{I}}_{\text{true}}, \mathbf{C}_{\text{goal}})$ .

We trained the module  $\mathcal{N}_{\text{syn}}$  to predict the final complete face image  $\mathbf{I}_1$  over a joint loss. The adversarial loss is defined as

$$\begin{aligned} \mathcal{L}_3 = & \mathbb{E}_{(\mathbf{I}_{\text{true}}, \mathbf{C}_{\text{fina}})} [\log D_2(\mathbf{I}_{\text{true}}, \mathbf{C}_{\text{goal}})] \\ & + \mathbb{E}_{(\mathbf{C}_{\text{fina}})} \log [1 - D_2(\mathbf{I}_1, \mathbf{C}_{\text{goal}})] \end{aligned} \quad (4)$$

The per-pixel loss is defined as follows

$$\mathcal{L}_4 = \frac{1}{S_m} \|\mathbf{I}_1 - \mathbf{I}_{\text{true}}\|_1 \quad (5)$$

which  $S_m$  denotes the size of the face mask  $\mathbf{I}_{\text{mask}}$  and  $\|\cdot\|_1$  denotes the  $L_1$  norm. Notice that we use the mask size  $S_m$  as the denominator to adjust the penalty.

The style loss ? computes the style distance between two face images as follows

$$\begin{aligned} \mathcal{L}_5 = & \\ & \sum_n \frac{1}{Q_n \times Q_n} \left\| \frac{G_n(\mathbf{I}_1 \odot (1 - \mathbf{I}_{\text{mask}})) - G_n(\hat{\mathbf{I}}_{\text{true}})}{Q_n \times H_n \times W_n} \right\|_1 \end{aligned} \quad (6)$$

where  $G_n(x) = \varphi_n(x)^T \varphi_n(x)$  denotes the Gram Matrix corresponding to  $\varphi_n(x)$ ,  $\varphi_n(\cdot)$  denotes the  $Q_n$  feature maps with the size  $H_n \times W_n$  of the  $n$ -th layer. In summary, the contour generator network  $\mathcal{N}_{\text{cont}}$  was trained with an objective comprised of an adversarial loss and feature-matching loss

$$\min_{G_1} \max_{D_1} \mathcal{L}_{G_1} = \min_{G_1} \left( \lambda_1 \max_{D_1} \mathcal{L}_1 + \lambda_2 \mathcal{L}_2 \right) \quad (7)$$

The total loss function of  $\mathcal{N}_{\text{syn}}$  follows

$$\min_{G_2} \max_{D_2} \mathcal{L}_{G_2} = \lambda_3 \max_{D_2} \mathcal{L}_3 + \lambda_4 \mathcal{L}_4 + \lambda_5 \mathcal{L}_5 \quad (8)$$

here, we set  $\lambda_1=1$ ,  $\lambda_2=11.5$ ,  $\lambda_3=0.1$ ,  $\lambda_4=1$  and  $\lambda_5=250$  respectively.

### 3.3. 3D Model Reconstruction

Since the face is a very standardized figure, we use a human face template to construct the basic shape (here, we adopt 3DMM) Paysan et al. (2009). Commonly, we describe single people’s face with PCA Blanz and Vetter (2003), where shape and texture are separated:

$$\begin{cases} \mathbf{S} = \bar{\mathbf{S}} + \mathbf{A}_{\text{id}}\alpha_{\text{id}} + \mathbf{B}_{\text{exp}}\beta_{\text{exp}} \\ \mathbf{T} = \bar{\mathbf{T}} + \mathbf{B}_{\text{te}}\beta_{\text{te}} \end{cases} \quad (9)$$

where  $\bar{\mathbf{S}}$  and  $\bar{\mathbf{T}}$  denote the average shape and texture,  $\mathbf{A}_{\text{id}}$ ,  $\mathbf{B}_{\text{exp}}$  and  $\mathbf{B}_{\text{te}}$  denote the PCA basis of shape (identity and expression) and texture.  $\alpha_{\text{id}} \in \mathbb{R}^{80}$ ,  $\beta_{\text{exp}} \in \mathbb{R}^{64}$  and  $\beta_{\text{te}} \in \mathbb{R}^{80}$  are the corresponding 3DMM coefficient vectors. After the 3D face is reconstructed, it can be projected onto the image plane with the perspective projection:

$$\mathbf{P}_{2\text{d}} = k * \mathbf{P}_{\text{p}} * \mathbf{R} * \mathbf{S}_{\text{mod}} + \mathbf{t}_{2\text{d}} \quad (10)$$

where  $\mathbf{P}_{2\text{d}}$  denotes the projection function that turned the 3D model into 2D face positions,  $k$  denotes the scale factor,  $\mathbf{P}_{\text{p}}$  denotes the projection matrix,  $\mathbf{R} \in SO(3)$  denotes the rotation matrix and  $\mathbf{t}_{2\text{d}} \in \mathbb{R}^3$  denotes the translation vector.

We approximated the scene illumination with Spherical Harmonics (SH) Ramamoorthi and Hanrahan (2001) parameterized by coefficient vector  $\gamma \in \mathbb{R}^9$ . Overall, the unknown vector parameters can be formulated  $\mathbf{V}_{\mathbf{x}} = (\alpha_{\text{id}}, \beta_{\text{exp}}, \beta_{\text{te}}, \gamma, \mathbf{p}) \in \mathbb{R}^{239}$ , where  $\mathbf{p} \in \mathbb{R}^6 = \{\text{pitch}, \text{yaw}, \text{roll}, k, \mathbf{t}_{2\text{D}}\}$  denotes face poses. Here, we used a revised ResNet-50 He et al. (2016) network to predict  $\mathbf{V}_{\mathbf{x}}$ . The corresponding loss function consists of two parts: pixel-wise loss and face feature loss.

*Per-pixel Loss.* The pixel loss function minimizes the difference between the input image  $\mathbf{I}_{\text{fina}}^{(j)}$  and the output image  $\mathbf{I}_{\text{y}}^{(j)}$ . The rendering layer renders back a rendered image  $\mathbf{I}_{\text{y}}^{(j)}$  to compare with the image  $\mathbf{I}_{\text{1}}^{(j)}$ . We compute the per-pixel loss with:

$$\mathcal{L}_6 = \left\| \mathbf{I}_{\text{1}}^{(j)} - \mathbf{I}_{\text{y}}^{(j)} \right\|_2 \quad (11)$$

where  $j$  denotes pixel index and  $\|\cdot\|_2$  denotes the  $L_2$  norm.

*Face Features Loss.* We introduce a loss function at the face recognition level to reduce the difference between the 3D model of the face and the 2D image. The loss function computes the feature difference between the input image  $\mathbf{I}_{\text{1}}$  and rendered image  $\mathbf{I}_{\text{y}}$ . We define the loss as a cosine distance:

$$\mathcal{L}_7 = 1 - \frac{\langle G(\mathbf{I}_{\text{1}}), G(\mathbf{I}_{\text{y}}) \rangle}{\|G(\mathbf{I}_{\text{1}})\| \cdot \|G(\mathbf{I}_{\text{y}})\|} \quad (12)$$

where  $G(\cdot)$  denotes the feature extraction function by FaceNet Schroff et al. (2015),  $\langle \cdot, \cdot \rangle$  denotes the inner product.

In summary, we used the loss function  $\mathcal{L}_{3D}$  to reconstruct the basic shape of the face. We set  $\mathcal{L}_{3D} = \lambda_6\mathcal{L}_6 + \lambda_7\mathcal{L}_7$ , where  $\lambda_6=1.4$  and  $\lambda_7=0.25$  respectively in all our experiments. We then used a coarse-to-fine graph convolutional network based on the frameworks of Lin et al. Lin et al. (2020) for producing the fine texture  $T_{\text{add}}$ .

## 4. Experimental Results

Figure 3 shows our experimental results compared with the others Chen et al. (2019). The result shows that our method is far superior to other frameworks. Our 3D reconstruction method can handle occluded scenes, such as palms, chains on the forehead, and glasses. Other frameworks can not handle occlusions well; they are more focused on the generation of high-definition textures.

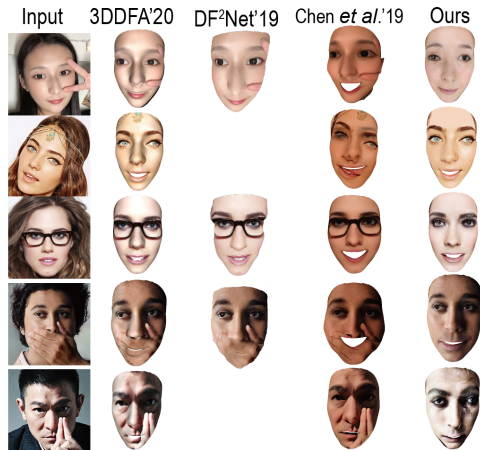


Figure 3: Comparison of qualitative results. Baseline methods from left to right: 3DDFA, DF2Net, Chen *et al.* , and our method. The blank area means that the corresponding method does not work.

## 5. Conclusions

In this study, we present an efficient 3D face reconstruction framework capable of functioning effectively in occluded environments. Given the wealth of domain knowledge and extensive prior research in the realm of human faces, we readily acquired relevant datasets. Our approach excels in estimating facial details even in areas where the face is obscured, such as by hands, forehead accessories, or glasses. Extensive experiments have conclusively demonstrated that our method significantly outperforms previous approaches in both accuracy and robustness.

## References

- Blanz, V., Vetter, T., 2003. Face recognition based on fitting a 3d morphable model. *IEEE Transactions on pattern analysis and machine intelligence* 25, 1063–1074.
- Cao, C., Hou, Q., Zhou, K., 2014. Displaced dynamic expression regression for real-time facial tracking and animation. *ACM Transactions on graphics (TOG)* 33, 1–10.
- Chen, A., Chen, Z., Zhang, G., Mitchell, K., Yu, J., 2019. Photo-realistic facial details synthesis from single image, in: *Proceedings of the IEEE International Conference on Computer Vision*, pp. 9429–9439.
- Dolhansky, B., Ferrer, C.C., 2018. Eye in-painting with exemplar generative adversarial networks, in: *Proceedings of the IEEE conference on computer vision and pattern recognition*, pp. 7902–7911.
- He, K., Zhang, X., Ren, S., Sun, J., 2016. Deep residual learning for image recognition, in: *Proceedings of the IEEE conference on computer vision and pattern recognition*, pp. 770–778.
- Iizuka, S., Simo-Serra, E., Ishikawa, H., 2017. Globally and locally consistent image completion. *ACM Transactions on Graphics (ToG)* 36, 1–14.
- Isola, P., Zhu, J.Y., Zhou, T., Efros, A.A., 2017. Image-to-image translation with conditional adversarial networks, in: *Proceedings of the IEEE conference on computer vision and pattern recognition*, pp. 1125–1134.
- Johnson, J., Gupta, A., Fei-Fei, L., 2018. Image generation from scene graphs, in: *Proceedings of the IEEE conference on computer vision and pattern recognition*, pp. 1219–1228.
- Jourabloo, A., Liu, X., 2016. Large-pose face alignment via cnn-based dense 3d model fitting, in: *Proceedings of the IEEE conference on computer vision and pattern recognition*, pp. 4188–4196.
- Karras, T., Laine, S., Aittala, M., Hellsten, J., Lehtinen, J., Aila, T., 2020. Analyzing and improving the image quality of stylegan, in: *Proceedings of the IEEE/CVF Conference on Computer Vision and Pattern Recognition*, pp. 8110–8119.
- Lee, C.H., Liu, Z., Wu, L., Luo, P., 2020. Maskgan: Towards diverse and interactive facial image manipulation, in: *Proceedings of the IEEE/CVF Conference on Computer Vision and Pattern Recognition*, pp. 5549–5558.
- Lin, J., Yuan, Y., Shao, T., Zhou, K., 2020. Towards high-fidelity 3d face reconstruction from in-the-wild images using graph convolutional networks. *arXiv preprint arXiv:2003.05653* .
- Pathak, D., Krahenbuhl, P., Donahue, J., Darrell, T., Efros, A.A., 2016. Context encoders: Feature learning by inpainting, in: *Proceedings of the IEEE conference on computer vision and pattern recognition*, pp. 2536–2544.
- Paysan, P., Knothe, R., Amberg, B., Romdhani, S., Vetter, T., 2009. A 3d face model for pose and illumination invariant face recognition, in: *2009 Sixth IEEE International Conference on Advanced Video and Signal Based Surveillance*, Ieee. pp. 296–301.

- Ramamoorthi, R., Hanrahan, P., 2001. An efficient representation for irradiance environment maps, in: Proceedings of the 28th annual conference on Computer graphics and interactive techniques, pp. 497–500.
- Schroff, F., Kalenichenko, D., Philbin, J., 2015. Facenet: A unified embedding for face recognition and clustering, in: Proceedings of the IEEE conference on computer vision and pattern recognition, pp. 815–823.
- Tuan Tran, A., Hassner, T., Masi, I., Medioni, G., 2017. Regressing robust and discriminative 3d morphable models with a very deep neural network, in: Proceedings of the IEEE Conference on Computer Vision and Pattern Recognition, pp. 5163–5172.
- Wei, Z., Sun, Y., Wang, J., Lai, H., Liu, S., 2017. Learning adaptive receptive fields for deep image parsing network, in: Proceedings of the IEEE conference on computer vision and pattern recognition, pp. 2434–2442.
- Yang, C., Lu, X., Lin, Z., Shechtman, E., Wang, O., Li, H., 2017. High-resolution image inpainting using multi-scale neural patch synthesis, in: Proceedings of the IEEE conference on computer vision and pattern recognition, pp. 6721–6729.
- Yin, Z., Yiu, V., Hu, X., Tang, L., 2021. End-to-end face parsing via interlinked convolutional neural networks. *Cognitive Neurodynamics* 15, 169–179.
- Yu, J., Lin, Z., Yang, J., Shen, X., Lu, X., Huang, T.S., 2018. Generative image inpainting with contextual attention, in: Proceedings of the IEEE conference on computer vision and pattern recognition, pp. 5505–5514.
- Zhou, L., Liu, Z., He, X., 2017. Face parsing via a fully-convolutional continuous crf neural network. arXiv preprint arXiv:1708.03736 .